Pressure Driven Ligand Rearrangement Reaction in a Cobalt−Chloride Complex

Ray Engelke,* Donald R. Pettit,[1] and Stephen A. Sheffield

Los Alamos National Laboratory, MS P952, Los Alamos, New Mexico 87545

Received: September 24, 1996; In Final Form: December 5, 1996[⊗]

We report experimental results concerning the occurrence and rate of the reaction $CoCl_2(EtOH)_2 + 4EtOH \rightarrow Co(EtOH)_6^{2+} + 2Cl^-$ induced by transient high pressure. The experimental probe used to interrogate the system was time-resolved visible light spectroscopy. The transient high pressures induced in the samples were produced by projectiles launched by a single-stage gas gun; consequently, the hydrodynamic flows experienced by the samples were well-defined. The pressures the test samples were subjected to were in the range 0.75−6.7 GPa. Ambient-pressure control experiments, in which the reaction was induced by altering sample temperature, are also reported. For a 20/80 wt % $CoCl_2 \cdot 6H_2O$/EtOH solution, shocked to ca. 6.7 GPa, we observed the disappearance of signature spectrum of the $CoCl_2(EtOH)_2$ species and the appearance of the spectrum of the $Co(EtOH)_6^{2+}$ structure. The cobalt structure on the left side of the equilibrium equation above is tetrahedral, while that on the right is octahedral. In shock-pressurized systems, we have observed the disappearance of the tetrahedral complex and found the time scale for this process is ca. 200 ns. Similarly, in other shock experiments, we have observed the appearance of the octahedral complex and found the time scale for this process is ca. 500 ns. The relevance of the present results to ideas concerning the character of ionic chemical reactions possibly important in detonating condensed-phase explosives is briefly discussed.

I. Introduction

We report broad-band visible-light spectroscopic observations on the chemical system $CoCl_2 \cdot 6H_2O$/EtOH shocked to high pressure. In the experiments to be discussed, the materials were all shocked from the liquid state. The shock pressurization was produced by use of projectiles from a single-stage gas gun; this allowed precise control of the hydrodynamic states experienced by the samples. The object of our experiments was to try to shift the equilibrium

$$CoCl_2X_2 + 4X \rightleftharpoons CoX_6^{2+} + 2Cl^- \qquad (1)$$

to the right by a rapid increase in pressure. The ligands in the $CoCl_2X_2$ complex are tetrahedrally arranged about the cobalt atom, whereas in the CoX_6^{2+} case, the arrangement is octahedral. In our case X was the ligand EtOH. If an equilibrium shift was observed, then we hoped to make an experimental determination of the rate of reequilibration.

It is known that static high pressure shifts equilibrium (1) to the right, due to the large increase in the concentration of electrically charged species produced in the rearrangement from the tetrahedral to the octahedral ligand complex. The system changes from one containing only electrically neutral species to one in which three of the species present carry a net charge.[2]

We have observed reaction (1) in systems shocked from 0.75 to 6.7 GPa. For systems shocked to ca. 6.7 GPa**,** the time constants for disappearance/appearance of the tetrahedral/octahedral complex are ca. 200/500 ns, respectively. These observations show that ligand rearrangements can occur rapidly in shocked solutions even when the ligands are quite large moieties such as ethanol molecules.

These results bear on ideas previously put forward on the possible importance of ionic species in the detonation chemical kinetics of some condensed-phase explosives. For example, there are indications that the ionic forms play an important role in the high-pressure chemical kinetics of the liquid explosive nitromethane and in other nitroalkanes with an "aci" form.[3] See section VI for further discussion of this.

II. Background

The study of temperature effects on the visible-light spectra of $CoCl_2$/alcohol complexes is quite old; see, e.g., ref 4 and references therein. This early work showed that blue to pink color changes occur in aqueous and alcoholic $CoCl_2$ solutions upon cooling. It was also shown that there are parallels between the observed effects in anhydrous alcohol and aqueous $CoCl_2$ solutions.

To our knowledge, the first reported work on static high-pressure effects on $CoCl_2$ solution spectra is that of Wick.[5] She did static high-pressure experiments (up to 0.15 GPa) on $CoCl_2/H_2O$ solutions. Her qualitative experiments showed that the color changes caused by increasing the temperature and increasing the pressure oppose each other; these observations are consistent with a chemical reaction that has a negative volume of reaction.

Later, Kitamura[2] thoroughly studied the effect of pressure (up to 0.3 GPa) on equilibrium (1). In his studies, X was (1) various primary alcohols and (2) one secondary alcohol. All the primary alcohols exhibited analogous behavior, indicating that a single type of reaction is occurring for this class of molecules. He also did electrical conductivity experiments and experiments in which equilibrium (1) was manipulated by addition of LiCl. His experiments give substantial support for the hypothesis that equilibrium (1) is actually the reaction being studied. Kitamura found very large negative volumes of reaction (ca. $-200 < \Delta V < -400$ cm^3/mol), when X is a primary alcohol (e.g., ethanol). Ishihara et al.[6] did a similar set of high-pressure experiments with X = acetone. Reference 7 contains observations of how one $CoCl_2$ peak of interest shifts as a function of static pressure in aqueous solution.

From the static high-pressure results on $CoCl_2$/alcohol systems cited above, it seemed likely that a situation favoring the right side of equilibrium (1) could be produced in a shock-wave experiment. Note, however, that in such an experiment the

[⊗] Abstract published in *Advance ACS Abstracts,* February 15, 1997.

S1089-5639(96)02940-4 CCC: $14.00

increased pressure (which favors the octahedral complex) is accompanied by an increased temperature (which favors the tetrahedral complex). It is worth considering the relative importance of these changes.

Suppose we consider equilibrium (1) as representing a two-level statistical mechanical system with the left side (tetrahedral form) and the right side (octahedral form) having occupation numbers of N_2 and N_1, respectively. We further assume that the temperature and pressure in the system have values T and P. Then

$$N_2/N_1 = \exp[-(\Delta E + P\Delta V)/kT] \quad (2)$$

where ΔE is the energy separating the two "states" and ΔV is the volume of reaction. The total differential of eq 2 can be written as

$$\mathrm{d}(N_2/N_1) = (kT)^{-1}(N_2/N_1)[\Delta E\,(\mathrm{d}T/T) - |\Delta V|\mathrm{d}P] \quad (3)$$

Note that the premultiplier on the squared bracketed term in eq 3 is positive definite. Therefore, the sign of the bracketed term determines the sign of $\mathrm{d}(N_2/N_1)$. Replacing the differentials in eq 3 by finite increments and assuming conservative values for T (=300 K), ΔT (=200 K), ΔE (=10 kcal/mol), ΔV (=−30 cm^3/mol), and ΔP (=2 GPa) shows that

$$\Delta(N_2/N_1) \cong -13(N_2/N_1)$$

Therefore, even with conservative assumptions, it appeared that a shock-wave experiment would produce conditions that would strongly favor the formation of the octahedral complex.

We chose to do the transient high-pressure experiments on the cobalt/EtOH complex rather than the methanol or the propanol complexes after obtaining broad-band absorption results from ambient-pressure experiments. The ethanol complex gave the best indications that we would be able to measure a transient high-pressure effect with our apparatus.

In the preliminary work we found that for the $CoCl_2$/EtOH tetrahedral and octahedral complexes the ratio of the molar absorption coefficients of their strongest bands is of the order of 10. Thus, it is significantly more difficult to observe the presence of the octahedral complex than the tetrahedral complex. This fact dictated how some of our cell thickness' and the $CoCl_2$ concentration of the cell contents were chosen. This will be discussed further below.

Our spectroscopic technique for detecting the tetrahedral and octahedral complexes was the observation of two broad bands with peaks at ca. 520 nm (octahedral) and 670 nm (tetrahedral). It is appropriate to describe briefly the microscopic origin of these bands. Ligand field theory shows that for a Co(II) atom in a tetrahedral ligand field, such as occurs in the tetrahedral complex $CoCl_2X_2$, the cobalt atom's 3d orbitals are split into a pair and triplet of orbitals with e and t_2 symmetry; the e orbitals have lower energies than the t_2 symmetry ones.[8] Similarly for the CoX_6^{2+} structure, where the ligand field has octahedral symmetry, the 3d orbitals split into a pair and a triplet of orbitals with e_g and t_{2g} symmetry; in this case, the t_{2g} orbitals have lower energy. In the ground state of a tetrahedral Co(II) complex, the two e orbitals each contain two electrons, while the three t_2 orbitals each contain one. For a Co(II) octahedral complex, the three t_{2g} orbitals contain five electrons and the two e_g orbitals contain one electron each. The bands observed in our spectra are from the spin-allowed transitions $^4A_2[e^4t_2^3] \rightarrow {}^4T_1(P)$ and $^4T_{1g}(F)$ $[t_{2g}^5e_g{}^2] \rightarrow {}^4T_{1g}(P)$ for the tetrahedral and octahedral complexes, respectively.

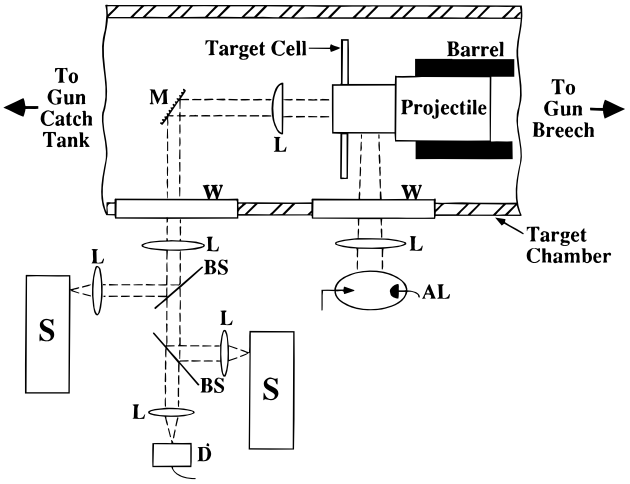

Figure 1. General layout of the experimental assembly; this figure is not drawn to scale. The following symbols are used in the figure: W = window, L = lens, M = mirror, BS = beam splitter, AL = arc lamp, S = spectrometer, and D = photodiode. The projectile enters from the right and strikes the target cell. After collision, light from the arc lamp passes once through the nose of the projectile and once through the sample in the target cell. The transmitted light is then optically manipulated out of the target chamber into the gun chamber bunker; it was then split into three beams and directed into two spectrometers and a photodiode. The target cell and projectile subsequently passed out of the target chamber and into the gun catch tank where they were stopped.

The reason the octahedral complex is favored strongly over the tetrahedral one in fluids subjected to high pressure is attributable to solvent "electrostriction". When an ion is created in a fluid of dipolar molecules, electrostriction occurs because electrostatic forces act to contract the solvent molecules surrounding the ion. The consequent volume reduction is energetically favored in a system subject to external pressure. One should note that the forces between an ion and a dipolar molecule are much stronger than the van der Waal forces that act between neutral molecules. Furthermore, the electrostatic force acts on many more solvent molecules because of its long range; this feature is accentuated in solvents with small dielectric constants. For a quantitative discussion of this effect see ref 9.

III. Experimental Apparatus, Techniques, and Materials

We used a single-stage light gas gun to produce the shock pressurization of our samples. Our gas gun can throw a 72.2 mm diameter projectile at speeds in the interval 0.25−1.45 mm/μs. Argon gas was used to drive the projectiles down the 10 m long barrel of the gun. The target chamber is evacuated to ca. 0.02 Torr to avoid experimental perturbations due to the presence of gas. Figure 1 is a simplified schema of a portion of the gun facility; it emphasizes the region near the target cell. Note this figure is not drawn to scale. The general layout of the optical system is also illustrated in the figure. The projectile speed at impact is measured to ca. 0.25% accuracy by use of electrical pins and digital oscilloscopes; this allows an accurate calculation of the initial shock state in the front window, provided its shock Hugoniot is known. Projectile "tilt" at impact is, typically, <1 mrad. These facts imply a well-defined (plane wave) flow field in the test sample, until the portion of the sample being spectroscopically probed is exposed to the rarefaction waves originating at the cell boundaries.

A detailed schema of the projectile nose and target cell is given in Figure 2. As shown, light from an Oriel 1000 W xenon arc lamp was fed into the projectile optical nose piece. It was turned 90° by a mirror within the nose assembly and then made

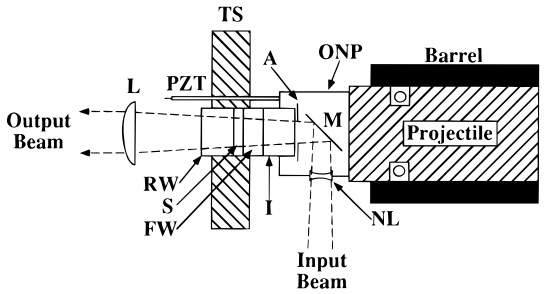

Figure 2. A more detailed drawing of the projectile optical nose assembly and the target cell. The following symbols are used in the drawing: NL = negative lens, M = mirror, ONP = optical nose piece, A = aperture, TS = target cell, FW = front window, S = sample, RW = rear window, PZT = piezoelectric pin, and L = lens. This figure shows how the arc lamp light was passed, once, through the cobalt chloride/ethanol sample. This figure is not drawn to scale.

one pass through the target cell. Because the projectile was designed in this way, it was important to monitor rotation of the projectile during its flight, since the amount of rotation affected the beam intensity experienced by the target solution. (More information on this aspect of the experiments is given below.) The light that traversed the cell was then collimated by a 100 mm focal length field lens, turned 90° by a mirror, and passed out of the target chamber through a fused silica window and into a collimating telescope. It then traveled ca. 3 m into the control room bunker, where it was optically manipulated and *f*# matched into two spectrometers and a photodiode.

The impactor window was a piece of Z-cut sapphire 31.75 mm diameter by 12 mm thick. The optical nose piece was a 38.1 mm diameter by 48 mm long black anodized aluminum cylinder. The diameter of the light beam entering the target cell was ca. 5 mm. A 12 mm diameter aperture was present to minimize stray light. The target cell windows consisted of Z-cut 31.75 mm diameter sapphire cylinders; the front (impactor side) window was 3 mm thick, while the rear one was 12 mm thick. A primary reason for choosing sapphire for the impactor and target windows is its well-studied shock-wave properties.[10] The cell windows were expoxied into a brass body; window separation (i.e., the sample thickness) was controlled by brass shims placed between the windows. The target cell had two filling ports; these were sealed with O-rings and screws and were vacuum-tight. The target cell assembly was held in place and perpendicular to the gun muzzle axis by an adjustable three-posted screw mount.

Four Spex spectrometers were mounted on an optical table in the control room. Two of these were *f*4/0.22 m instruments with 150 line pairs/mm gratings, while the other two were *f*6/0.5 m instruments with 300 line pairs/mm gratings. Two spectrometers were used in any given experiment. The spectra were gathered by two Tracor Northern optical multichannel analyzers. These consisted of a 25 mm diameter intensifier tube coupled to a cooled 1024-channel diode array; in most of our experiments an intensifier gain of 4000 was used. Slit widths used in the experiments were always 100 μm wide, except in shot 785 (see Table 1) where one spectrometer used a 200 μm wide slit.

The projectile can rotate in the gun barrel in its travel from the gun breech to the target cell. Rotation of the projectile modifies the intensity of the light beam that gets from the lamp to the photodiode and spectrometers. Therefore, a method was needed to measure the projectile rotation. This was done by having the metal periphery of the projectile collide with a vertical stainless steel wire immediately before the collision of the impactor with the target cell. The amount of rotation during the projectile's flight was then measured from the mark on the recovered projectile. A negative 25 mm focal length lens (see Figure 2) was mounted in the side of the optical nose piece. This lens reduces the dependence of the output light intensity on projective rotation. For example, the worst projectile rotation encountered was ca. 12°; such a rotation reduced the intensity received at the spectrometer by about a factor of 2. Furthermore, before each dynamic experiment, several static spectroscopic reference spectra were taken with the projectile (in contact with the target cell) rotated over a set of angles. The samples used for the reference spectra were 4.81/95.19 wt % H_2O/EtOH. The static run whose rotation angle was closest to the measured rotation angle in the dynamic experiment was used as the reference spectrum for that experiment.

A portion of the light beam was split off before entry into the spectrometers and focused onto a silicon photodiode. This photodiode gave a time-resolved measurement of the total light intensity passing through the target cell as a function of time.

A fiducial pulse for timing various experimental events was obtained from a piezoelectric pin placed on the target cell periphery; this pin was actuated by the collision of the projectile with the target.

The chemicals used in the experiments were as follows. EM Science reagent grade cobalt(ous) chloride hexahydrate was used as received from the manufacturer, except in the some of the control experiments where only sample temperature was varied; in these experiments we used this material in a dehydrated form. The dehydrated material was obtained by heating the hydrated material in an oven at 170° for ca. 48 h. USI Chemical 200-proof punctilious ethanol was dehydrated by use of Type 3A molecular sieve (that was freshly oven dried) before it was used in the experiments. In the preparation of the EtOH/H_2O reference solutions used to determine absorbancies in the absence of any cobalt chloride, EM Science glass-distilled OmniSolv water was added in an amount equivalent to the water of hydration in a 10.1/89.9 wt % $CoCl_2 \cdot 6H_2O$/EtOH solution.

IV. Results

(A) Temperature Variation Experiments. We began our sequence of experiments with a survey study of the visible light absorption spectra of $CoCl_2 \cdot 6H_2O$ dissolved in various concentrations of water, methanol, ethanol, and propanol at ambient pressure. It was found that $CoCl_2 \cdot 6H_2O$/EtOH solutions were the ones in which we could most easily manipulate the tetrahedral to octahedral equilibrium shift, when temperature was varied. Both anhydrous $CoCl_2$/EtOH solutions and $CoCl_2 \cdot 6H_2O$/EtOH solutions were investigated. The difference in the absorption spectra of such solutions was measurable, but slight. Because of this, we used the hydrated material in the high-pressure experiments.

We found that, in the thin sample cells (ca. 200−300 μm thick) to be used in most of the shock-wave experiments, we needed to use ca. 10 wt % $CoCl_2 \cdot 6H_2O$ to get an acceptable amount of absorption by the tetrahedral complex. An ethyl alcohol solution of this type contains ca. 4.55 wt % H_2O. A benefit of using the hydrated material was that unavoidable traces of absorbed atmospheric moisture did not affect our solutions—as it possibly would anhydrous ones. Figure 3 shows measured absorbancies of a 10.07/89.93 wt % $CoCl_2 \cdot 6H_2O$/EtOH solution at various temperatures. The sample cell used in this experiment was 303 μm thick. This cell was eventually used in a shock-wave experiment (i.e., shot 785; see Table 1 and below). The temperature variation was produced by bathing the cell in liquid nitrogen, until it reached ca. −57 °C; it was

TABLE 1: Experimental Parameters

experiment type/shot no.[a]	solution composition (wt %)[b]	sample thickness (μm)	press. (GPa)[c]	temp (°C)	gate time from shock entry (ns)[d]	wavelength range (nm)[e]
temp control experiment	10.07/89.93	303	ambient	varied from −57 to 0		(365−535)//(530−700)
thin cell/ring-up						
shot 757	10.07/89.93	193	6.5	200/200	859/875	(365−535)//(530−700)
shot 758	10.07/89.93	195	0.4/3.5−5.8	25−90/120−160	96/330	
solvent control ring-up experiment						
shot 759	4.81/95.19 wt % H_2O/EtOH	125	6.4	190/190	859/875	(365−535)//(530−700)
thick cell/single shock						
shot 780	10.07/89.93	2202	0.75	80/80−110	844/978	(268−765)//(266−751)
thin cell/ring-up						
shot 785	20.00/80.00	303	6.7	160/165	886/1095	(424−671)//(266−751)

[a] "Ring up" experiments are those in which the final pressure was achieved by multiple shocking of the sample during the reverberation process. In the "single-shock" experiment, the final pressure achieved during the diagnostic period was produced by a single shock. [b] The material composition is written here as $CoCl_2 \cdot 6H_2O$/EtOH wt %, except for shot 759. [c] The calculated pressure at the middle particle of the sample at gate time; see footnote *d*. [d] Gate time is defined as the time from shock entry into the sample to the center of the intensifier gate interval. Entries are for spectrometer 1/spectrometer 2. The gate time widths for the two spectrometers were always 118 and 150 ns, respectively. [e] Wavelength range for which data were taken with spectrometers 1 and 2, respectively.

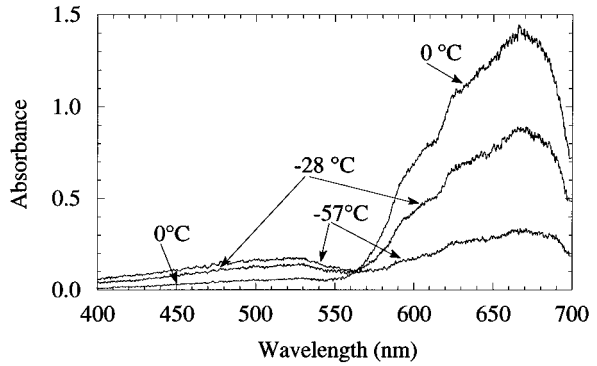

Figure 3. Static spectra as a function of temperature. The 10.07/89.93 $CoCl_2 \cdot 6H_2O$/EtOH solution was spectroscopically probed when the sample was at −57, −28, and 0 °C. These experiments indicate that the molar absorbance of the tetrahedral complex is roughly 10 times that of the octahedral form; however, note that at −57 °C there is still some tetrahedral complex present.

then allowed to warm to room temperature by not replenishing the liquid nitrogen in the bath. During the warmup period, spectra were taken at every 4 °C increase in temperature, until the cell reached 0 °C. In taking these spectra, an average gate time of 134 ns was used on the intensifiers. The spectra shown in Figure 3 are averages obtained by gating the spectrometers approximately 20 times; the coadded spectra were all obtained within about ca. 30 s. The coadding was done to improve the signal-to-noise ratio of the data.

The band that peaks at ca. 670 nm in Figure 3 is due to absorption by the tetrahedral complex. As the figure clearly shows, this species is favored by high temperature. One should also note a second weaker band with a peak at ca. 520 nm. This peak is due to the octahedral complex, which is favored by low temperature. The data in Figure 3 show that the ratio of the absorption coefficients of the tetrahedral complex to the octahedral complex is roughly 10 (=1.5/0.15), under these conditions. Consequently, it is much easier to detect the presence of the tetrahedral complex.

(B) Shock-Wave Experiment Preliminaries and Flow Calculations. Before describing the spectra obtained from the shocked cobalt chloride/ethanol solutions, we will discuss some of the fluid-mechanical processes that occur in the experiments.

When a projectile strikes a target cell, a shock wave is sent forward into the target cell front sapphire window (see Figure 2). The shock passes through the 3 mm thick sapphire window and reaches the cobalt chloride/ethanol sample in ca. 261 ns. At this point, a shock is sent into the sample solution, and a rarefaction is reflected back into the sapphire window. Eventually, the shock in the sample solution reaches the sapphire rear window, where it produces a shock in this window and a reflected shock traveling back toward the sapphire front window. The pressures as a function of time experienced by the first, middle, and last "particles" in three different experiments are shown quantitatively in Figure 4.

Calculations of the sort displayed in Figure 4 were done to simulate the shock processes in the $CoCl_2$ solutions during the ring-up process between the sapphire front and back windows. The CTH wave code was chosen for doing the calculations.[11] CTH is a mixed Eulerian/Lagrangian code. That is, the problem is setup in the Eulerian frame and then mapped to the Lagrangian frame where the fluid motion is calculated for one time step. The results are then mapped back into the Eulerian frame. This process is then repeated for the next time step. This methodology eliminates some of the problems associated with cell distortion, etc., experienced with pure Eulerian codes. All the calculations were done on an HP 735 workstation.

All the calculations assumed one-dimensional flow and used a Mie−Gruneisen equation of state with a constant specific heat and a constant value of the Gruneisen parameter divided by specific volume. The equations of state for the various sample types were developed by using the universal liquid Hugoniot form.[12] This form depends only on the initial mass density and the ambient pressure sound speed of a liquid; it has been shown to apply remarkably well to essentially all liquids.[13] We experimentally determined the sound speeds and mass densities for our various sample types (see Table 2). Using these values, a Hugoniot was constructed and then least squares fitted to the quadratic Hugoniot form available in the CTH code.

Constant values for the specific heat at constant volume and the Gruneisen parameter were determined using thermodynamic identities and available data for ethanol.[14] Although the analogous parameters for the $CoCl_2$ solutions would be expected to differ somewhat from these values, these differences are not expected to greatly affect the computed values of the mechanical variables (e.g., pressure and density). They are expected to affect the thermal data considerably, but there is currently no good way to measure and calibrate the temperatures in shock

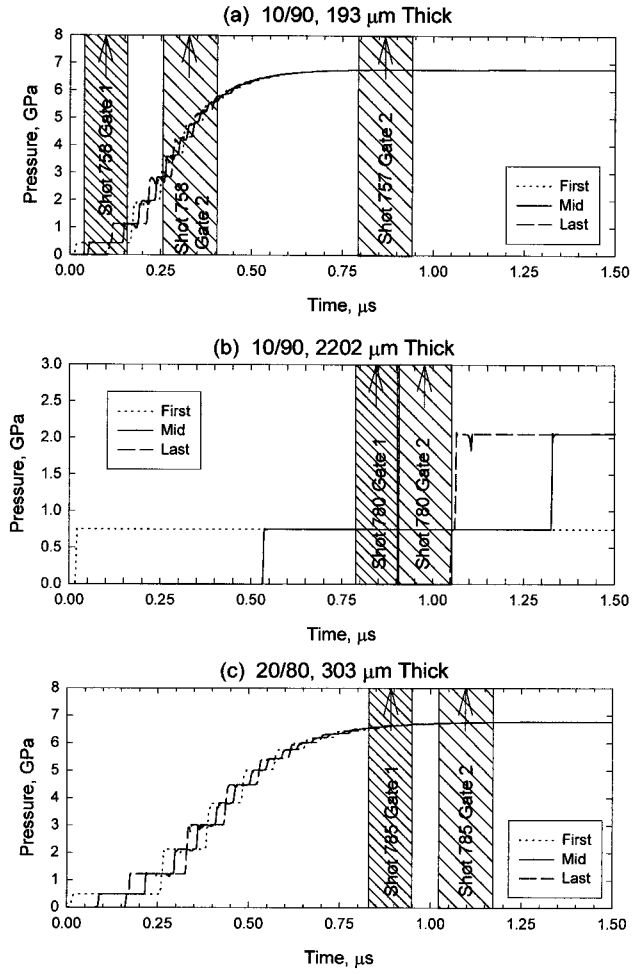

Figure 4. Calculated pressure−time histories for the $CoCl_2 \cdot 6H_2O$/EtOH solutions. The following processes are depicted: (a) the ring-up process of a 10/90 wt % solution in a 193 μm thick cell, (b) the single-shock process of a 10/90 wt % solution in a 2202 μm thick cell, and (c) the ring-up process of a 20/80 wt % solution in a 303 μm thick cell. Zero time in all cases is the time the initial shock enters the solution. Gate time and widths are shown in each panel of the figure by shaded boxes with different shades for each spectrometer; the center of the gate intervals is indicated by upward pointing arrows. First, middle, and last indicate particles at these positions in the sample.

TABLE 2: Mass Densities and Sound Speeds

composition (wt %) $CoCl_2 \cdot 6H_2O$/EtOH	mass density (g/cm^3)	sound speed ($mm/\mu s$)
0/100	0.780 at 26.6 °C	1.150 at 24.3 °C
10.07/89.93	0.835 at 26.6 °C	1.183 at 24.5 °C
20.00/80.00	0.897 at 26.4 °C	1.222 at 24.6 °C

experiments; we think that the *relative* temperatures predicted by our procedure are reasonable representation of reality.

The pressure/time histories shown in Figure 4 represent a sample's fluid-mechanical state until rarefaction waves arrive from the test cell's boundaries. For the geometry of our cells, the time for edge rarefactions to reach the region of the sample being probed optically was ca. 1200 ns. Until this time, the flow in the sample was one-dimensional. All the spectra in our experiments were taken before side rarefaction entry. This avoided the complexities of interpreting data from flows that were multidimensional.

The descriptions produced by these numerical calculations aided and improved our interpretation of the experimental data described next.

(C) Thin-Cell Ring-Up Experiments. In the first shock-wave experiments to be described the sample cells were "thin".

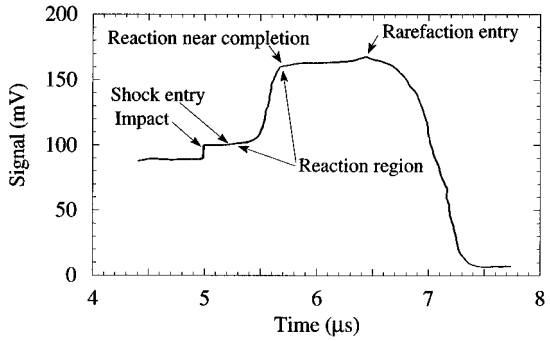

Figure 5. A white-light photodiode record. The Fresnel reflection losses for sapphire are about 7.7% per surface with an additional 1% scattering loss per surface due to the 60/40 scratch/dig surface polish. The elimination of two surfaces when the projectile contacts the target, therefore, produces about a 17% increase in optical transmission. This event provides an absolute time fiducial. The shock transit time through the front target cell window can be calculated from the known shock properties of sapphire; this gives the shock entry time into the sample. Optical transmission is seen to increase during the reaction process due the disappearance of the strongly absorbing tetrahedral complex. A sudden change in optical transmission indicates near completion of the tetrahedral to octahedral equilibrium shift. At about 1200 ns after shock entry into the sample, radial rarefactions begin to disassemble the target cell and, consequently, the signal rapidly decreases. Axial rarefactions enter after the radial ones because of the window thickness.

Here thin means that many shock reverberations could occur within the sample before rarefactions from the cell boundaries caused the fluid flow in the sample area being optically probed to become multidimensional. Specifically "thin" here means our samples were ca. 300 μm thick or less.

Other parameters of interest in all the shock-wave experiments were (1) the initial sample temperatures were within the range 25 ± 4 °C, (2) the gate widths of spectrometers 1 and 2 were 118 and 150 ns, respectively, and (3) the projectiles were thrown at close to 0.30 mm/μs, except in shot 780 where a speed of 0.45 mm/μs was used.

Figure 5 is an example of a white-light photodiode record obtained in one of the experiments. The following events are evident on this record. First, a signal increase occurs due to the disappearance of two sapphire surfaces at the moment of collision of the projectile with the front window of the sample cell (see figure caption); this event provides an optical time fiducial for the remainder of the experiment. (Note this jump in intensity is not due to a "flash" of light produced by the collision (e.g., by gas compression), since a flash would appear as a pulse on the intensity record and not as a step.) The known shock properties of sapphire and the projectile speed allow one to calculate the shock transit time through the sapphire front window (ca. 261 ns). The optical fiducial and this transit time allow the time for shock entry into the sample to be marked in Figure 5. Second, after the sample is shocked, one notes an increasing light signal that is attributable to the disappearance of the strongly absorbing tetrahedral cobalt chloride/EtOH complex; i.e., a time interval is evident on the record during which the new equilibrium is being established. Third, at approximately 1200 ns after shock entry into the sample, the rarefactions from the cell boundaries arrive and begin to destroy the test cell; this, in turn, begins to decrease the light intensity received at the photodiode.

Figure 6 shows spectroscopic data collected from two thin cell experiments (shots 757 and 758) in the wavelength range 550−700 nm. These experiments were nominally identical in cell thickness, in projectile speed, and in the 10.1/89.9 wt % $CoCl_2 \cdot 6H_2O$/EtOH solution they contained (see Table 1). The parameter examined was the gate time at which spectroscopic

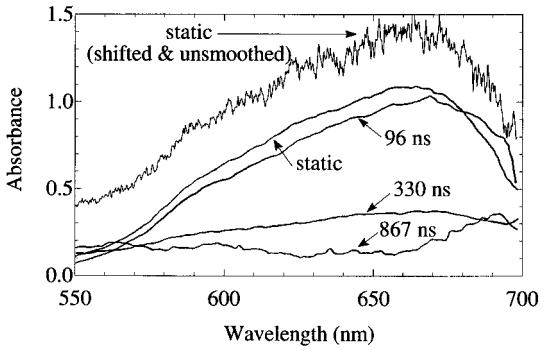

Figure 6. Data showing the disappearance of the tetrahedral complex from thin-cell ring-up shots 757 and 758. The time-resolved disappearance of the tetrahedral complex is indicated by the disappearance of the broad absorption band centered at ca. 660 nm. The data have been smoothed using a five-point moving average. An example of the noise present on the signals before smoothing is shown on the shifted and unsmoothed static spectrum. The growth of absorption by the octahedral complex is not evident because of its significantly smaller molar absorbance.

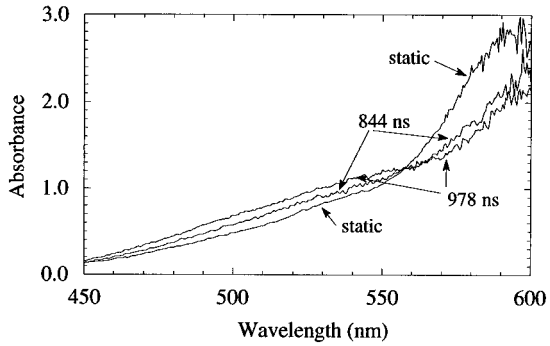

Figure 7. Data illustrating the depletion of the tetrahedral complex obtained from a thick-cell single-shock experiment (shot 780). The absorption is dominated by the tetrahedral complex, and this masks the growing in of the weak absorption due to the octahedral complex. There is an isosbestic point at about 560 nm.

data were taken (see the shaded boxes in Figure 4). The gate times used were 96, 330, and ca. 867 ns; see the arrows in Figure 4a. The data at 867 ns is the average of two sets of data taken at 859 and 875 ns. Static spectra were also taken before the shock experiments. As can be seen in the figure, all three dynamic experiments show a reduced absorbance due to the tetrahedral complex; spectra at later gate times show a larger diminution of the tetrahedral absorbance. As can be seen from Table 1 and Figure 4a, it is not clear that this diminution is only a function of time, since in the 96 and 330 ns records the sample cell was not completely "rung up". The "middle" particle of the sample was between 0 and 0.4 GPa during essentially all of the 96 ns gate data (shot 758) and between 3.0 and 5.8 GPa during the 330 ns gate data (shot 758). The calculated temperature of the middle particle of the sample during the 96 and 330 ns gate intervals varied from 25 to 90 °C and 120 to 160 °C, respectively. The temperature of the sample material during the 859 and 875 ns gate intervals was ca. 200 °C (shot 757).

The data in Figure 6 are strong evidence that, for a cell of this type rung up to 6.5 GPa and spectroscopically analyzed 867 ns after shock entry into the test sample, the tetrahedral complex's presence has been essentially eliminated. Furthermore, the shocking of the sample does not appear to broaden or shift the tetrahedral complex band substantially.

As a control experiment, we did a ring-up experiment that contained only water and ethanol (shot 759). In this experiment a 4.81/95.19 wt % H_2O/EtOH solution was shocked in a cell that was 125 μm thick. This relative weight of water to ethanol was chosen to produce the same relative number of water to ethanol molecules as was present in the experiments that utilized the 10.1/89.9 wt % $CoCl_2 \cdot 6H_2O$ solution. The purpose of the experiment was to demonstrate that the solvent molecules were not producing any features in our spectra, under shock conditions, that we were interpreting as being due to the cobalt chloride complexes. The two spectra, both taken ca. 867 ns after the shock entered the sample, show an essentially constant absorbance of 0.3 ± 0.1 over the wavelength range 460−680 nm. The pressure in the sample during data acquisition was ca. 6.4 GPa. This experiment demonstrates that the absorbance spectra due to the solvent molecules is not of concern in our interpretation of the cobalt chloride complex spectra.

(D) Thick-Cell Single-Shock Experiment. One is uneasy about making an interpretation of an underlying phenomenon based solely on the disappearance of a signal. Therefore, in an attempt to strengthen our interpretation, we wished to perform a shock experiment that showed the appearance of the octahedral spectral band along with the disappearance of the band due to the tetrahedral complex. This led us to do a shock experiment with a much increased cell thickness. We hoped to compensate for the low absorbance of the octahedral complex by this change in cell geometry. A penalty caused by this change is that the cell can no longer be allowed to ring up to high pressure before taking data. This is because the shock transit time across the 2202 μm wide cell we used is approximately the same as the time for side rarefaction entry into the optically sampled region. Therefore, data can only be obtained from a sample that has been shocked one time. We compensated for this somewhat by throwing the projectile at higher speed. However, there is a limitation here also, since sapphire undergoes an elastic/plastic transition at ca. 12.5 GPa, which strongly reduces the amount of light it will transmit. We wanted to stay well below this pressure in the sapphire and so used a projectile speed of 0.45 mm/μs; this produced a single-shock pressure in the 10.1/89.9 wt % $CoCl_2 \cdot 6H_2O$/EtOH sample of 0.75 GPa. This value is to be compared to the 6.5 GPa achieved when spectra were taken in shot 757. Note, however, that a benefit is that the reduced pressure in the single-shock experiment allows one to probe the pressure dependence of the equilibrium shift to some degree by comparing with data taken in the ring-up experiments.

Figure 7 shows static data and data obtained from the single-shock experiment (shot 780). Note that this figure is truncated at 600 nm because, with the thick cell geometry, we were outside the effective dynamic range of our instrument at the tetrahedral band peak. Even at 600 nm, the spectra show significant noise due to dynamic range limitations. Spectrometer 2 was gated so that it began taking a spectrum immediately after spectrometer 1 finished (see Figure 4b and Table 1). The spectrometer 2 data include absorbance information almost up to the time when the shock struck the rear window.

The spectra shown in Figure 7 order properly in the light of the tetrahedral to octahedral equilibrium shift. That is, the absorbancies on the tetrahedral band shoulder (600 nm) in the static, 844 ns, and 978 ns spectra are ca. 2.7, 2.3, and 2.1. This is evidence of a decrease in the amount of tetrahedral complex present in the optical path. In contrast, at the position of the octahedral complex band peak (520 nm), the absorbancies at the same times are ca. 0.7, 0.8, and 0.9, respectively. This is evidence of an increased presence of the octahedral complex along the optical path.

While suggestive of the process we were searching for, these data still do not present an indisputable case. It does, however, suggest that for material shocked to ca. 0.75 GPa the rate of

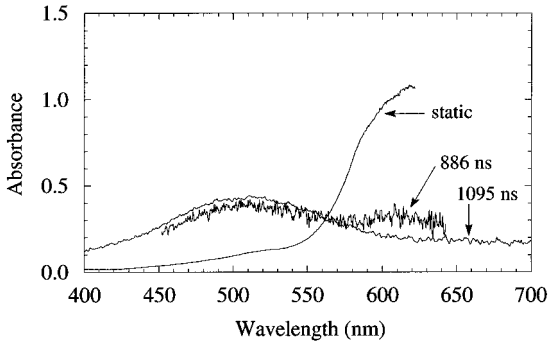

Figure 8. Data illustrating the growing in of the octahedral complex as obtained from a thin-cell ring-up experiment (shot 785). This shot was constructed specifically to show the appearance of the octahedral complex following the disappearance of the tetrahedral form. The broad absorption band centered at ca. 510 nm is due to octahedral complex absorption. The static absorbance of the tetrahedral complex at 660 nm exceeded the dynamic range of the spectrograph−detector system and is truncated at 620 nm. There is an isosbestic point at ca. 560 nm.

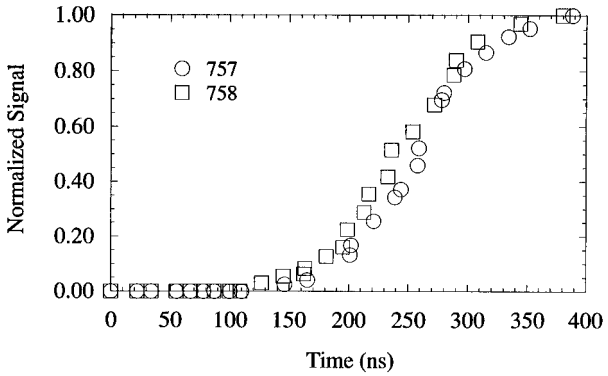

Figure 9. White-light photodiode records from thin-cell ring-up shots 757 and 758. The reaction zone region is normalized to the point defined by the plateau at the end of the rapid transmission change (see Figure 5). The time scale shown begins 100 ns before shock entry into the cell. If it is assumed that the white-light optical transmission is dominated by the disappearance of the tetrahedral complex at early times, these curves show a continuous time history of the disappearance of the tetrahedral complex over the first 300 ns in which the sample was shocked; in contrast, the spectroscopic data shown in Figure 6 only show this phenomenon at four discrete times. Sigmoid curves $y = (1 + \exp[-(t - m_1)/m_2)])^{-1}$ fit the data with an R values of 0.998. The parameter value (m_1, m_2) pairs for shots 757 and 758 are (157 ns, 29.7 ns) and (142 ns, 34.7 ns), respectively. The point of rapid change (inflection point) occurs ca. 150 ns after shock entry into the sample.

the equilibrium shift is significantly slower than when the sample is pressurized to much higher pressure. For example, compare the decrease in absorbance at 600 nm in Figure 6 (at time = 867 ns) with that in Figure 7 (at time = 844 ns). In the ring-up experiment (Figure 6), where a pressure of 6.5 GPa had been reached when data were taken, essentially no tetrahedral complex remains after 867 ns. In contrast, in the single-shock experiment (Figure 7), only a small decrease in absorbance has occurred at approximately the same time (847 ns). We conclude from this that one can speed up the rate of equilibration strongly by increasing the pressure well above 0.75 GPa. Note that the shock temperatures of the samples cannot account for this observation. As shown in Table 1, the sample temperatures in shots 757 and 780, during the time data were taken, were ca. 200 and ≤110 °C, respectively. Consequently, the tetrahedral complex was favored by the temperature present in the shot 757 sample.

(E) Thin-Cell Ring-Up Experiment with Higher Concentration Sample. Since the thick cell experiment described above was not completely successful in producing unambiguous evidence for the appearance of the octahedral complex when the tetrahedral complex disappears, another approach was tried in the hope of achieving this end. Because the single-shock experiment indicated that the rate of equilibration was enhanced at pressures higher than 0.75 GPa, we returned to a ring-up (i.e., thin) type cell. To increase the amount of absorbance by the octahedral complex, we doubled the concentration of the $CoCl_2$ in solution; i.e., we used a 20.00/80.00 wt % $CoCl_2 \cdot 6H_2O$/EtOH solution. Additionally, the cell thickness was increased from ca. 200 to 303 μm.

As shown by Figure 4c, a cell this thick requires ca. 800 ns to ring up to 95% of maximum pressure. Therefore, spectrometers 1 and 2 were gated data 886 and 1095 ns, respectively. The gate at 1095 ns is near the time region where side rarefactions are beginning to effect the sample region viewed. This was accepted because we wished to probe the sample as late as possible so that the time for reequilibration was maximized. The projectile was thrown at a speed of 0.30 mm/μs in this experiment. The pressure and temperature in the sample at gate time were ca. 6.7 GPa and 160−165 °C, respectively.

Figure 8 shows the experimental results from shot 785. Three spectra are shown; i.e., a static and the two dynamics. In the static, the absorbance of the tetrahedral complex above 620 nm was beyond the dynamic range of our instrument because of the higher solution concentration and the increased cell thickness. Another feature to note on the static is that there is a hint of an absorption feature at ca. 520 nm embedded in the left shoulder of the strong band with a peak at 670 nm. This is due to the ambient concentration of the octahedral complex. The two spectra taken of the shocked sample show the disappearance of the tetrahedral form and the appearance of the absorption band of the octahedral form (band peak at ca. 510 nm).

This experiment demonstrates that when a $CoCl_2 \cdot 6H_2O$/EtOH solution is shock pressurized to ca. 6.7 GPa, the tetrahedral/octahedral complex equilibrium is shifted strongly in favor of the octahedral complex.

(F) Analysis of the Reequilibration Rate. Clearly, the spectral data from shots 757, 758, and 785 (see Figures 6 and 8) contain information concerning the rate of the tetrahedral to octahedral reequilibration process.

To motivate the idea that a rate analysis of this data is worthwhile, we begin by indicating the reproducibility of the experiments. Figure 9 shows superposed white-light photodiode records from shots 757 and 758. Considering the complexity of the experiments and of the phenomena being studied, the two records show satisfactory similarity. One might suppose that the photodiode records themselves could be used for a rate analysis. This is not so since (1) the data on the records is a superposition of light received at all visible wavelengths and cannot be correlated simply with either the tetrahedral or the octahedral complex and (2) the sensitivity of the photodiode was wavelength dependent and, consequently, requires a deconvolution process even to get back to the true white-light signal. Therefore, we base our analysis on the spectral data shown in Figures 6 and 8.

Even using these data requires simplifying assumptions, since during a ring-up process, the sample goes through a manifold of thermodynamic states. However, a simplifying factor is that above a certain pressure (which is probably less than 2 GPa) further increases in pressure are not effective (or are only weakly effective) in increasing the rate of equilibration or in shifting the equilibrium concentration of the complexes. This is due to the decreasing compressibility of the fluid as the pressure is

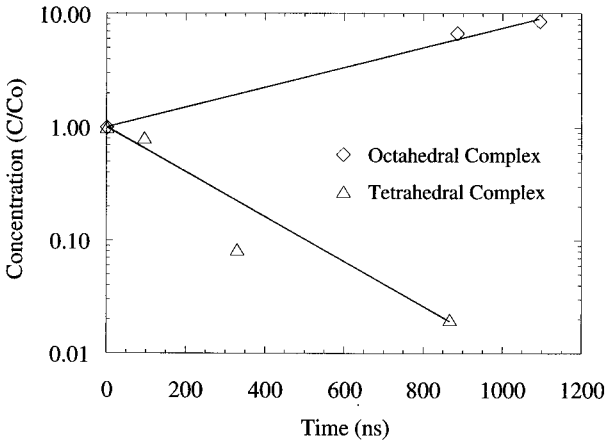

Figure 10. Plot of the relative concentrations vs reaction time for the disappearance of the tetrahedral complex (using shots 757 and 758) and the growth of the octahedral complex (using shot 785).

increased to very high values.[15] Hence, we assume that, during the times when data were taken in shots 757, 758, and 785, the reequilibration rate was at its asymptotically high value because of the late gate times used; i.e., during the time intervals when spectral data were taken, the samples were at very high pressure. Therefore, we assume the whole data set can be considered as arising from a sample at a common pressure, and the only relevant independent variable that the species concentration depends on is the time difference from shock entry into the sample to the center of the gate interval. One set of data does not fit this picture; i.e., the data taken at 96 ns in shot 758. We shall comment on this further below. We also assume that the concentrations of the tetrahedral and octahedral complexes are proportional to the measured absorbancies at the band peaks. This corresponds to an assumption of the validity of Beer's law and of the pressure independence of the molar extinction coefficients at the band peaks. (We did not experimentally validate these assumptions, although the isosbestic point evidence discussed below supports the second assumption.) Then, the ratio of the static absorbances with those from the dynamic experiments gives us the concentration of a complex relative to its initial value (C/C_0) as a function of time (see Figure 10). It is implicit in this treatment that we can properly normalize out the difference in absolute concentration of the cobalt structures resulting from the use of the 10.1/89.9 wt % solution in shots 757 and 758 and the 20.0/80.0 wt % solution used in shot 785 by normalizing to the static absorbance.

The reduced data, plotted in the semilog plane (Figure 10), show an approximate exponential dependence of species concentration on time. Least-squares fits of this data to the form $y = \exp(t/\tau)$ gave τ values of -220 ± 61 and $+500 \pm 21$ ns for the reequilibration times of the tetrahedral and octahedral, respectively; the error estimates are one standard deviation. Since the final concentration value for the tetrahedral complex was zero within our experimental resolution, the best fit parameters were obtained by iterating the final value near zero until the best fit correlation coefficient was obtained. The final value of C/C_0 for the tetrahedral complex obtained in this way was 0.02. The correlation coefficients of the two fits were 0.974 and 0.989 for the tetrahedral and octahedral complexes, respectively. Note that the tetrahedral complex C/C_0 value obtained in shot 758 at 96 ns is ca. -0.16 units above the regression line; this is probably due to the low pressure in the sample at this time and the consequent high concentration of the tetrahedral complex due to the longer time constant of the reequilibration process at low pressure.

The disappearance of the tetrahedral complex occurs ca. 2.3 times faster than the growth of the octahedral complex. We hypothesize that the difference between the two rates is the result of the time it takes for the four additional EtOH molecules to move into position and then properly arrange themselves about the cobalt ion before the octahedral absorbance pattern is observed.

V. Conclusions and Discussion

In this work we have found the following: (1) by use of shock waves with a strength as low as 0.75 GPa, it is possible to shift equilibrium (1), i.e., to reduce the concentration of the tetrahedral complex $CoCl_2(EtOH)_2$ and enhance the concentration of the octahedral form $Co(EtOH)_6^{2+}$; (2) when the process is driven by higher pressure (e.g., ca. 6.5 GPa), equilibrium (1) can be driven very far to the right (as shown by the data in Figures 6 and 8); (3) the time-resolved spectra of the shocked systems allow some insight into the rate constants involved in the reequilibration process; (4) our analysis shows that, at ca. 6.5 GPa and 160−200 °C, the tetrahedral complex disappearance has exponential time dependence with a time constant of -220 ± 61 ns; (5) the appearance of the octahedral complex does *not* occur at the same rate as the disappearance of the tetrahedral form; (6) the appearance of the octahedral form occurs with exponential dependence, but with a time constant of $+500 \pm 21$ ns; (7) items (4) and (6) of the current list are evidence that there are intermediate processes involved in reestablishing equilibrium (1); and (8) we conjecture that these processes are the production of the $Co(EtOH)_n$ ($2 < n < 6$) species that are precursors to the octahedral complex.

One further feature of the data needs to be discussed. Note that there are isosbestic points in Figures 3, 7, and 8. One way such a point can occur at a wavelength λ is if the sum of the areal number density of the tetrahedral and octahedral complexes is constant and if the molar absorption coefficients of the two complexes at λ are equal. The condition on the sum of the concentration holds in a two-component system at equilibrium. One sees from Figure 3 that, at ambient pressure, our system has an isosbestic point at ca. 555 nm. In Figures 7 and 8, one similarly sees isosbestic points at ca. 558 and 563 nm, respectively.

We hypothesize the following explanation for the latter two observations. In the thick-cell single-shock experiment (shot 780, Figure 7), the equilibrium had not been driven strongly off its ambient-pressure value because of the low pressure generated by the single shock. Furthermore, the data were taken at late times (≥844 ns). Thus, much of the shocked sample had sufficient time to reequilibrate to tetrahedral/octahedral concentrations required by the local pressure—giving the isosbestic point.

In shot 785 (Figure 8), the thin cell was rung up to near its final pressure and held for ca. 300 ns before data were taken (at ≥886 ns); therefore, the material in this sample had sufficient time to nearly reequilibrate before the major portion of the data were taken.

In contrast, in the ring-up experiment (shot 758) where data were taken at early times, the absorbances for the 96 and 330 ns spectra do not cross the static absorbance spectrum; i.e., there is no isosbestic point present on the data from this shot. We conjecture that this is due to the spectra from this shot being taken at times similar to the rate process time scales obtained in the rate analysis. Consequently, the system was significantly out of equilibrium, and the sum of the tetrahedral and octahedral complex concentrations was not constant due to the two distinct rate constants involved.

The existence of the isosbestic point in Figure 8 indicates that the molar absorption coefficients of the tetrahedral and

octahedral complexes at wavelengths in the vicinity of ca 560 nm are not significantly pressure dependent up to pressures of ca 6.5 GPa.

The main thrust of work at our laboratory is the study of properties of highly energetic materials. One working hypothesis we have developed over the years via phenomenological studies is that ionic reaction mechanisms may be important first steps in the exothermic chemistry of some explosives, e.g., nitromethane [CH_3NO_2] and some other nitroalkanes. For example, there exists experimental evidence that (1) high static pressure increases the presence of the nitromethane aci ion $[CH_2NO_2]^-$,[3b] (2) high static pressure causes nitromethane to be a more sensitive explosive,[16a] and (3) increased concentration of the aci ion causes nitromethane to be a more sensitive explosive.[3a,16b] These observations point to the ionization reaction $CH_3NO_2 \rightarrow [CH_2NO_2]^- +$ solvated $[H^+]$ being important in the early detonation kinetics of nitromethane.

As a beginning of the spectroscopic studies of such mechanisms, we thought it would be instructive to examine such a process in a nonenergetic material. This led to the present work which shows that ionic rearrangements of large ligands can be produced by transient high pressure and that such transformations can be observed with our spectroscopic system. The observed ionic rearrangement reactions in $CoCl_2$/EtOH solutions are quite rapid (200−500 ns) considering the complexity of the reactions and the size of the EtOH ligands. It is likely that the proton transfer reactions we suspect are important in the nitroalkane exothermic reactions will be very much faster and, consequently, will be more difficult to study.

Acknowledgment. This work was supported by the U.S. Department of Energy. We also thank R. L. Rabie for his interest in and support of this project.

References and Notes

(1) Present address: NASA-JSC, Mail Code CB, Houston, TX 77058.

(2) Kitamura, Y. *Rev. Phys. Chem. Jpn.* **1969**, *39*, 1.

(3) (a) Engelke, R.; Earl, W. L.; Rohlfing, C. M. *Int. J. Chem. Kinet.* **1986**, *18*, 1205. (b) Engelke, R.; Schiferl, D.; Storm, C. B.; Earl, W. L. *J. Phys. Chem.* **1988**, *92*, 6815.

(4) Donnan, F. G.; Basset Jr., H. *J. Chem. Soc.* **1902**, *81*, 939.

(5) Wick, F. G. *Am. Acad. Arts. Sci. Proc.* **1923**, *58* , 557.

(6) Ishihara, I.; Kimihiki, H.; Osugi J. *Rev. Phys. Chem. Jpn.* **1974**, *44*, 11.

(7) Fyfe, W. S. *J. Chem. Phys.* **1962**, *37*, 1894.

(8) (a) Cotton, F. A.; Wilkinson, G. *Advanced Inorganic Chemistry, A Comprehensive Text*; 4th ed.; Wiley: New York, 1980; pp 770−773. (b) Cotton, F. A. *J. Chem. Educ.* **1964**, *41*, 466.

(9) Isaacs, N. S. *Liquid Phase High Pressure Chemistry*; Wiley: New York, 1981; pp 99−101.

(10) Barker, L. M.; Hollenbach, R. E. *J. Appl. Phys.* **1970**, *41*, 4208.

(11) McGlaun, M. C.; Thompson, S. L.; Kmetyk, L. N.; Elrick, M. G. A Brief Description of the Three-Dimensional Shock Wave Physics Code CTH, Sandia National Laboratories, SAND89-0607, 1989.

(12) Woolfolk, R. W.; Cowperthwaite, M.; Shaw, R. *Thermochim. Acta* **1973**, *5*, 409.

(13) Sheffield, S. A.; Alcon, R. R. In *Shock Compression of Condensed Matter−1989*; Schmidt, S. C., Johnson, J. N., Davison, L. W., Eds.; Elsevier: New York, 1989; pp 683−686.

(14) (a) *CRC Handbook of Chemistry and Physics*; Lide, D. R., Ed.; CRC Press: New York, 1995. (b) *American Institute of Physics Handbook*; Billing, B. H., et al., Eds.; McGraw-Hill: New York, 1963.

(15) le Noble, W. J. In *High Pressure Chemistry and Biochemistry*; Van Eldik, R., Jonas, J., Eds.; Reidel: Boston, 1987; p 298.

(16) (a) Lee, E. L.; Sanborn, R. H.; Stromberg, H. D. *Fifth Symposium (International) on Detonation*; Jacobs, S. J., Ed.; Office of Naval Research: Washington, DC, 1970; p 331. (b) Engelke, R. *Phys. Fluids* **1980**, *23*, 875.